CHARACTERISTICS OF CYLINDRICAL MULTICONDUCTOR TRANSMISSION LINES ABOVE A PERFECTLY CONDUCTING GROUND PLANE

O. D. Khan, A. Z. Elsherbeni, C. E. Smith, and D. Kajfez

1.   Introduction

The non-planar microstrip lines are becoming increasingly pop-
ular due to its wide range of applications which require circuits to
conform to curved surfaces such as those of aircraft, missiles, probes,
etc. The non-planar microstrip line studied here consists of a finite
number of infinitesimally thin perfectly conducting strips, placed ei-
ther between a dielectric substrate and an overlay, or on top of two
layers of dielectric substrates. The whole structure is then placed on
the tip of a perfectly wedge as shown in Figure 1. The quasi-TEM
characteristics of this geometry are rigorously derived, based on the
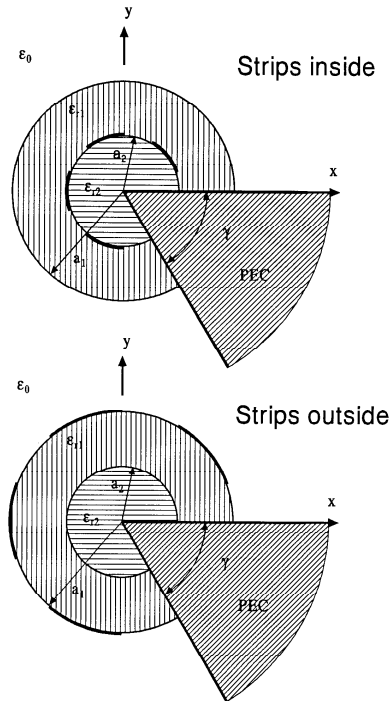technique presented in [1,2].

**Figure 1. The general configuration of the cylindrical multilayered multi-
conductor microstrip transmission line placed on a perfectly conducting
wedge (not to scale).**

The first part of this analysis is to determine the capacitance matrix for the multiconductor line. Once the capacitance matrix is obtained, other parameters such as the phase velocities, the characteristics impedances, and the coupling between the conductors are readily obtained from the capacitance matrix [3].

The derivation starts with solving Laplace's equation for the potentials in the free space region and in each of the dielectric region. with unknown expansion coefficients for each region. The expressions for the potentials are constructed such that the continuity of the tangential components of the electric field across the dielectric interfaces are automatically enforced. The remaining boundary conditions are applied by enforcing the potential to have constant voltages on the conducting strips and satisfying the jump discontinuity in the normal derivative of the potential across the dielectric interfaces. The equations obtained are then solved using Galerkin's method to find the expansion coefficients [2]. The expressions for the charge distributions on the strips and the capacitance matrix are then obtained. The transmission line considered for analysis consists of two cylindrical layers of dielectric material, the substrate and the overlay. The substrate is defined by permittivity ϵ_{r2} and radius a_2. The overlay is defined by permittivity ϵ_{r1} and radius a_1. The conducting strips are placed either on the interface between the substrate and the overlay or on top of the overlay as shown in Figure 1. The arc width of the strips is given by $(\beta_i - \alpha_i)^\circ$, where $i = 1, 2, \cdots, S$ and S is the total number of strips not counting the ground plane. The dielectric layers are placed on top of a perfectly conducting wedge of angle γ. Numerical results are presented for the phase velocities (difference in phase velocities between the various modes), the coupling coefficient (and coupling capacitances), the mode impedances, and the field distribution of the multiconductor cylindrical transmission line.

2.   Formulation

2.1. Potential expressions

In this section, the exact potential distributions inside and outside the dielectric regions are derived by satisfying Laplace's equation. In

free space region, we have

$$\nabla^2 V_o(\rho, \phi) = 0, \qquad \rho \geq a_1, \qquad 0 \leq \phi \leq 2\pi - \gamma \qquad (1)$$

subject to the boundary conditions, $V_o(a_1, \phi) = \Phi_1(\phi)$, at $0 \leq \phi \leq 2\pi - \gamma$ and $V_o(\rho, 0) = V_o(\rho, 2\pi - \gamma) = 0$, at $\rho \geq a_1$, where, $\Phi_1(\phi)$ is the potential on the interface at $\rho = a_1$ which is to be expressed in terms of Fourier series expansion with a set of unknown coefficients.

The potentials must be both finite and continuous everywhere and regular at infinity. The solution to Laplace's equation can be obtained using the method of separation of variables, that is

$$V_o = \sum_{n=1}^{\infty} A_n^{\circ} (\frac{a_1}{\rho}) \sin(n\Psi\phi), \qquad \Psi = \frac{\pi}{2\pi - \gamma} \qquad (2)$$

Similarly, in the dielectric regions, the potentials are found by solving Laplace's equation in their respective regions. In the outer dielectric region (the overlay), we have

$$\nabla^2 V_1(\rho, \phi) = 0, \qquad a_2 \leq \rho \leq a_1, \qquad 0 \leq \phi \leq 2\pi - \gamma \qquad (3)$$

subject to the following boundary conditions, $V_1(a_1, \phi) = \Phi_1(\phi)$, at $0 \leq \phi \leq 2\pi - \gamma$, $V_1(\rho, 0) = V_1(\rho, 2\pi - \gamma) = 0$, at $a_2 \leq \rho \leq a_1$, $V_2(a_2, \phi) = \Phi_2(\phi)$, at $0 \leq \phi \leq 2\pi - \gamma$, where $\Phi_1(\phi)$ is the potential on the interface at $\rho = a_1$ which is to be expressed in terms of a Fourier series expansion with a set of unknown coefficients. The solution to Laplace's equation in this region is then given by,

$$V_1 = \sum_{n=1}^{\infty} [A_n^1 (\frac{\rho}{a_2})^{n\Psi} + B_n^1 (\frac{a_1}{\rho})^{n\Psi}] \sin(n\Psi\phi) \qquad (4)$$

Finally, the potential in the inner dielectric region (the substrate) must satisfy,

$$\nabla^2 V_2(\rho, \phi) = 0, \qquad 0 \leq \rho \leq a_2, \qquad 0 \leq \phi \leq 2\pi - \gamma \qquad (5)$$

subject to the following boundary conditions, $V_2(a_2, \phi) = \Phi_2(\phi)$, at $0 \leq \phi \leq 2\pi - \gamma$, and $V_2(\rho, 0) = V_2(\rho, 2\pi - \gamma) = 0$, at $0 \leq \rho \leq a_2$, where $\phi_2(\phi)$ is the potential on the interface at $\rho = a_2$ which is to be expressed in terms of a Fourier series expansion with a set of unknown

coefficients. The solution of Laplace's equation in this region is then given by,

$$V_2 = \sum_{n=1}^{\infty} A_n^2 (\frac{\rho}{a_2})^{n\Psi} \sin(n\Psi\phi) \qquad (6)$$

2.2. Application of the boundary conditions

At the interface between different regions the potentials are continuous. Thus at the interface $\rho = a_1$ and $0 \leq \phi \leq 2\pi - \gamma$, we have $V_o(\phi) = V_1(\phi)$, and at $\rho = a_2$ and $0 \leq \phi \leq 2\pi - \gamma$ we have $V_1(\phi) = V_2(\phi)$. The potentials on the interfaces $\rho = a_1$ and $\rho = a_2$ are defined by the functions Φ_1 and Φ_2, respectively, as follows,

$$\Phi_1 = \sum_{m=1}^{\infty} \nu_{1m} \sin(m\Psi\phi), \qquad \Phi_2 = \sum_{m=1}^{\infty} \nu_{2m} \sin(m\Psi\phi) \qquad (7)$$

where ν_{1n} and ν_{2n} are unknown expansion coefficients. Using the above boundary conditions and the orthogonality of $\sin(m\Psi\phi)$ function, the expressions for the exact potentials in the three regions are then given by

$$V_0 = \sum_{n=1}^{\infty} \nu_{1n} (\frac{a_1}{\rho})^{n\Psi} \sin(n\Psi\phi), \quad \rho > a_1 \quad (8)$$

$$V_1 = \sum_{n=1}^{\infty} \left\{ [\frac{\nu_{2n} - \nu_{1n}R^{n\Psi}}{1 - R^{2n\Psi}}](\frac{\rho}{a_2})^{n\Psi} + [\frac{\nu_{1n} - \nu_{2n}R^{n\Psi}}{1 - R^{2n\Psi}}](\frac{a_1}{\rho})^{n\Psi} \right\} \cdot$$
$$\sin(n\Psi\phi), \qquad a_1 > \rho > a_2 \quad (9)$$

$$V_2 = \sum_{n=1}^{\infty} \nu_{2n} (\frac{\rho}{a_2})^{n\Psi} \sin(n\Psi\phi), \quad a_2 > \rho \quad (10)$$

where $R = a_1/a_2$. The above expressions for the potential distribution in the three regions were obtained in such a way that the continuity of the potentials across the dielectric interfaces and the continuity of the electric field [7, Sect. 3-2], are automatically satisfied.

Now, two additional boundary conditions need to be satisfied. The first of these conditions is the constant potential (or zero tangential electric field) on the strips. When the strips are placed between the substrate and the overlay, this condition is given below as follows,

$$\Phi_2 = \sum_{n=1}^{\infty} \nu_{2n} \sin(n\Psi\phi) = V_s, \qquad \alpha_s \leq \phi \leq \beta_s, \qquad s = 1, 2, 3, \cdots S$$

$$(11)$$

where, α_s and β_s are the beginning and ending angles of the strips.

The second condition that needs to be satisfied is that the normal component of the displacement vector $(\mathbf{D} = \epsilon\mathbf{E} = -\epsilon\nabla V)$ across each dielectric interface be discontinuous by an amount equal to the surface free charge density σ_s on the strips at that boundary.

Thus at the interface $\rho = a_1$, and with the strips placed between the substrate and the overlay, the following boundary condition must hold

$$\epsilon_o\epsilon_{r1}\frac{\partial V_1(\rho,\phi)}{\partial\rho} - \epsilon_o\frac{\partial V_o(\rho,\phi)}{\partial\rho} = 0, \qquad 0 \le \phi \le 2\pi - \gamma \qquad (12)$$

Similarly at the interface $\rho = a_2$, the following boundary condition must hold

$$\epsilon_{r2}\frac{\partial V_2(\rho,\phi)}{\partial\rho} - \epsilon_{r1}\frac{\partial V_1(\rho,\phi)}{\partial\rho} = \frac{1}{\epsilon_o}\sigma_s(\phi), \qquad on\ the\ strips$$
$$= 0, \qquad\qquad elsewhere \qquad (13)$$

where, $\sigma_s(\phi)$ is the charge distribution on strip s.

2.3. Solution of the expansion coefficients

The unknowns ν_{1n} and ν_{2n} are solved from Equations (11) through (13) by first replacing V_1, V_2, and V_3 in Equations (12) and (13) by their expressions from Equations (8) to (10) and then using Galerkin's procedure, i.e., testing with "$\sin(m\Psi\phi)$" and, integrating both sides from zero to "$2\pi - \gamma$". After some simplification a matrix equation is obtained for the case of strips placed between the substrate and the overlay as follows

$$\mathbf{S_{mn}}|\nu_{1m}\rangle = |V_m\rangle \qquad m = 1, 2, \cdots S \qquad n = 1, 2, \cdots S \qquad (14)$$

where, $\mathbf{S_{mn}}$ is a square matrix for the system of equation, $|\nu_{1m}\rangle$ is the vector of unknown potentials and $|V_m\rangle$ is the known forcing function vector. The elements of these matrices are

$$S_{mn} = n\Psi[(\epsilon_p - \epsilon_{r_1}F_8(n))F_7(n)F_3(m,n)) + \\ \epsilon_{r_1}F_9(n)F_3(m,n) + F_7(n)F_4(m,n)] \qquad (15)$$

$$V_m = \sum_{s=1}^{S} V_s G_s(m) \qquad (16)$$

where,

$$F_3(m, n) = \int_0^{\alpha_1} g(\phi)d\phi + \int_{\beta_1}^{\alpha_2} g(\phi)d\phi + \cdots + \int_{\beta_S}^{2\pi-\gamma} g(\phi)d\phi,$$

$$F_4(m, n) = \int_{\alpha_1}^{\beta_1} g(\phi)d\phi + \int_{\alpha_2}^{\beta_2} g(\phi)d\phi + \cdots + \int_{\alpha_S}^{\beta_S} g(\phi)d\phi,$$

$$F_7(n) = \frac{1 + R^{2n\Psi}}{2R^{n\Psi}} - \frac{\epsilon_p}{\epsilon_{r_1}}[\frac{1 - R^{2n\Psi}}{2R^{n\Psi}}], \quad \epsilon_p = 1$$

$$F_8(n) = \frac{1 + R^{2n\Psi}}{1 - R^{2n\Psi}}, \qquad F_9(n)\frac{2R^{n\Psi}}{1 - R^{2n\Psi}}$$

$$g(\phi) = \sin(n\Psi\pi)\sin(m\Psi\pi), \qquad G_s(m) = \int_{\alpha_s}^{\beta_s} \sin(m\Psi\phi)d\phi$$

From the matrix Equation (14), the unknown ν_{1m} is obtained. The other set of unknown ν_{2m} is obtained as $\nu_{2m} = \nu_{2m}/F_7$. Similarly, for the case of strips placed on top of the overlay, a matrix equation can be obtained by substituting ν_{1m} by ν_{2m}, and ϵ_p by ϵ_{r2} in Equation (15).

2.4. Total charge and the capacitance matrix

The total charge on the strips can be obtained from Equation (13) by applying Gauss's law and using the potential expansion functions that is

$$Q_s = \sum_{n=1}^{\infty} n\Psi[\epsilon_{r_2}\nu_{2n} - \epsilon_{r_1}(\nu_{2n}F_8(n) - \nu_{1n}F_9(n))] \int_{\alpha_s}^{\beta_s} \sin(n\Psi\phi)d\phi \quad (17)$$

Once the total charges on each strip is computed, the capacitance matrix can be obtained from the following equation:

$$Q_s = V_s C_{ss} + \sum_{\substack{k=1 \\ k \neq s}}^{S} C_{sk}(V_s - V_k) \tag{18}$$

The capacitance matrix is obtained by solving for S equations simultaneously corresponding to S strips and for each of these strips, a potential of 1 Volt is set on the sth strip while all other strips are set at zero potential [3]. In this way a square capacitance matrix of order

S is obtained with self capacitances denoted by C_{ss} and coupling capacitances denoted by C_{sk}.

2.5. Electric field distribution

The modes on the multiconductor line could be visually shown by plotting the electric field distribution around the transmission lines. The electric field can be obtained from the gradient of the potentials. In the free space region the field components are then given by

$$E_{x0} = \sum_{n=1}^{\infty} \nu_{1n}(\frac{a_1}{\rho})^{n\Psi}[(\frac{-n\Psi}{\rho})\sin(n\Psi\phi)\cos\phi - \frac{1}{\rho}n\Psi\cos(n\Psi\phi)\sin(\phi)]$$

(19a)

$$E_{y0} = \sum_{n=1}^{\infty} \nu_{1n}(\frac{a_1}{\rho})^{n\Psi}[(\frac{-n\Psi}{\rho})\sin(n\Psi\phi)\sin\phi + \frac{1}{\rho}n\Psi\cos(n\Psi\phi)\cos(\phi)]$$

(19b)

while in the substrate region the field components are

$$E_{x2} = \sum_{n=1}^{\infty} \nu_{2n}(\frac{\rho}{a_2})^{n\Psi}[(\frac{n\Psi}{\rho})\sin(n\Psi\phi)\cos\phi - \frac{1}{\rho}n\Psi\cos(n\Psi\phi)\sin(\phi)]$$

(20a)

$$E_{y2} = \sum_{n=1}^{\infty} \nu_{2n}(\frac{\rho}{a_2})^{n\Psi}[(\frac{n\Psi}{\rho})\sin(n\Psi\phi)\sin\phi + \frac{1}{\rho}n\Psi\cos(n\Psi\phi)\cos(\phi)]$$

(20b)

and in the overlay region the field components are

$$E_{x1} = \sum_{n=1}^{\infty} (\frac{n\Psi}{\rho})[(\frac{\nu_{2n} - \nu_{1n}R^{n\Psi}}{1 - R^{2n\Psi}})(\frac{\rho}{a_2})^{n\Psi} - (\frac{\nu_{1n} - \nu_{2n}R^{n\Psi}}{1 - R^{2n\Psi}})(\frac{a_1}{\rho})^{n\Psi}].$$
$$\sin(n\Psi\phi)\cos\phi$$
$$- \frac{1}{\rho}\sum_{n=1}^{\infty} n\Psi[(\frac{\nu_{2n} - \nu_{1n}R^{n\Psi}}{1 - R^{2n\Psi}})(\frac{\rho}{a_2})^{n\Psi} - (\frac{\nu_{1n} - \nu_{2n}R^{n\Psi}}{1 - R^{2n\Psi}})(\frac{a_1}{\rho})^{n\Psi}].$$
$$\cos(n\Psi\phi)\sin\phi$$

(21a)

$$E_{y1} = \sum_{n=1}^{\infty} (\frac{n\Psi}{\rho})[(\frac{\nu_{2n} - \nu_{1n}R^{n\Psi}}{1 - R^{2n\Psi}})(\frac{\rho}{a_2})^{n\Psi} - (\frac{\nu_{1n} - \nu_{2n}R^{n\Psi}}{1 - R^{2n\Psi}})(\frac{a_1}{\rho})^{n\Psi}].$$
$$\sin(n\Psi\phi)\sin\phi$$
$$- \frac{1}{\rho}\sum_{n=1}^{\infty} n\Psi[(\frac{\nu_{2n} - \nu_{1n}R^{n\Psi}}{1 - R^{2n\Psi}})(\frac{\rho}{a_2})^{n\Psi} - (\frac{\nu_{1n} - \nu_{2n}R^{n\Psi}}{1 - R^{2n\Psi}})(\frac{a_1}{\rho})^{n\Psi}].$$
$$\cos(n\Psi\phi)\cos\phi$$

(21b)

3.   Multiconductor Transmission Line Parameters

Once the capacitance matrix has been obtained, other transmission line parameters such as the characteristic impedances of individual conductors, the phase velocities, and the coupling coefficients can be obtained based on the multiconductor transmission line theory presented in [3].

3.1. Computation of voltage and current eigenvectors

The procedure to compute the impedance matrix and the phase velocities of the multiconductor line requires finding the voltage and current eigenvalues and eigenvectors. The following is a brief procedure for computing the impedance matrix and mode velocities. This is accomplished by computing the capacitance matrix twice, once with the line containing the original dielectric layers present, and then the second time with all dielectric layers replaced by free space. For all that follows, bold capital letters represent square matrices unless otherwise specified. First an electric induction coefficient matrix $\mathbf{K}$ is computed from the capacitance matrix whose elements are given by

$$K_{ii} = \sum_{j=1}^{S} Cij, \qquad Kij = -C_{ij}$$

Next, the inductance matrix $\mathbf{L}$, can be obtained by substituting free space for dielectric materials and running the same program which computes the capacitance matrix. This time the electric induction coefficient matrix can be denoted by $\mathbf{K}'$, so that $\mathbf{L}^{-1} = c^2\mathbf{K}'$. The eigenvalues λ_i, and eigenvectors $|x_i>$ for the matrix $\mathbf{L}^{-1}$ are defined by

$$\mathbf{L}^{-1}|x_i> = \lambda_i|x_i> \tag{22}$$

Next, a square matrix $\mathbf{G}$ is formed, from the eigenvectors $|x_i>$ as its columns $\mathbf{G} = (|x_i> \cdots |x_N>)$. The matrix $\mathbf{G}$ is orthogonal and real, such that, $\mathbf{G}^T = \mathbf{G}^{-1}$, and can be used to diagonalize $\mathbf{L}^{-1}$ as follows

$$\mathbf{G^T L^{-1} G} = diag.(\lambda_1, \lambda_2, \cdots, \lambda_N) = \mathbf{\Lambda} \tag{23}$$

Since the eigenvalues λ_i are positive and real, a diagonal square-root matrix $\mathbf{\Lambda}^{-1/2}$ can be defined as follows

$$\mathbf{\Lambda}^{-1/2} = diag.(\sqrt{\lambda_1}, \sqrt{\lambda_2}, \cdots, \sqrt{\lambda_N}) \tag{24}$$

A real symmetric matrix $\mathbf{B}$ is then defined as $\mathbf{B} = \mathbf{\Lambda}^{-1/2}\mathbf{G}^T\mathbf{KG}\mathbf{\Lambda}^{1/2}$. Its eigenvectors are defined by

$$\mathbf{B}|t_i> = \frac{1}{\nu_i^2}|t_i> \tag{25}$$

where ν_i are the phase velocities of the propagating modes on the line. These are the natural modes of the multiconductor transmission line in the sense that each mode can exist and propagate along the line independent of other modes. Finally, using the quantities obtained above, the voltage eigenvector is constructed as

$$|e_i> = \sqrt{\nu_i}\mathbf{G}\mathbf{\Lambda}^{-1/2}|t_i> \tag{26}$$

Similarly, the current eigenvector can be obtained as

$$|i_i> \frac{1}{\sqrt{\nu_i}}\mathbf{G}\mathbf{\Lambda}^{1/2}|t_i> \tag{27}$$

Voltage and current eigenvectors form a bi-orthogonal set $<e_i|i_j> = \delta_{ij}$, where δ_{ij} is a Kronecker delta.

3.2. Characteristic and mode impedances

A voltage mode matrix $\mathbf{M_V}$ is then defined as a square matrix, consisting of columns of voltage eigenvectors, that is

$$\mathbf{M_V} = (|e_1> \cdots \cdots |e_N>) \tag{28}$$

such that the characteristic impedance matrix is obtained from the matrix product of $\mathbf{M_V}$ and its transpose

$$\mathbf{R_c} = \mathbf{M_V}\mathbf{M_V^T} \tag{29}$$

The current and voltage eigenvectors are related to each other by the circuit relationship $|e_j> = \mathbf{R_c}|i_j>$.

It is sometimes useful to define the characteristic impedances of individual conductors of the multicondutor line. This method of defining the characteristic impedances was used by Matthaei *et.al* [4]. They define the characteristic impedances Z_{0i}^j as the ratio of the voltage on conductor j to the current on conductor j when a wave of the mode i travels along the line, that is

$$Z_{0i}^j = \frac{e_{ji}}{i_{ji}} = \frac{<u_j|\mathbf{R_c}|i_i>}{<u_j|i_i>} \tag{30}$$

where $< u_j|$ is a row vector which contains zeros in all its columns except for the jth conductor under consideration.

4.   Numerical Results

The equations derived in previous sections were used to analyze up to four conducting strips placed on the substrate or on the overlay. The purpose of this analysis is to establish conditions under which the cylindrical transmission system under study exhibits the least phase distortion and minimum crosstalk.

4.1. Geometry of the transmission line

Three configurations of the transmission line are analyzed, namely the two-strip, three-strip and four-strip cases. Furthermore, each configuration was studied for the strips outside and strips inside cases. In all cases the wedge angle γ is set to $180\,^{\circ}$, so that the transmission line system is a semi-cylindrical structure with a planar ground plane. Figure 2 shows the four-strip configuration of the transmission line model used for numerical analysis.
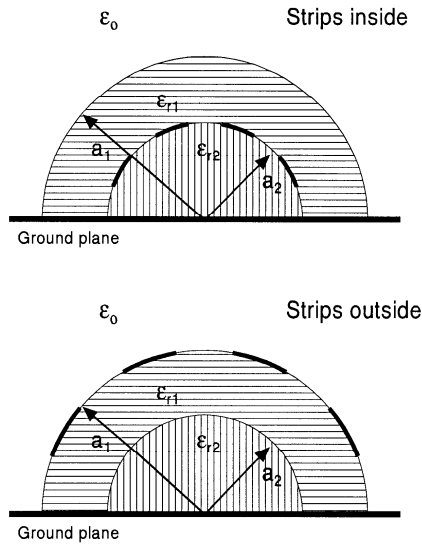

Figure 2. Geometries of the cylindrical four conductor transmission lines with $\gamma = 180°$ (not to scale).

4.2. Reliability of numerical results

To establish the reliability of the numerical results in the absence of verification from literature, a convergence test was performed. The behavior of the self and mutual capacitances was investigated as the order of the matrix N was increased. The capacitance matrix is the basis from which other numerical results were obtained using the multiconductor line theory. The convergence of the capacitances is an important factor in establishing the reliability of the results that will be later obtained. In Figure 3 the normalized capacitances for the four-strip transmission line are plotted as a function of $1/N$. It is observed that the percentage error (relative to the extension of the curve) is about 8% when the order of the matrix is 100. It reduces to about 2% when the order of the matrix is 500.
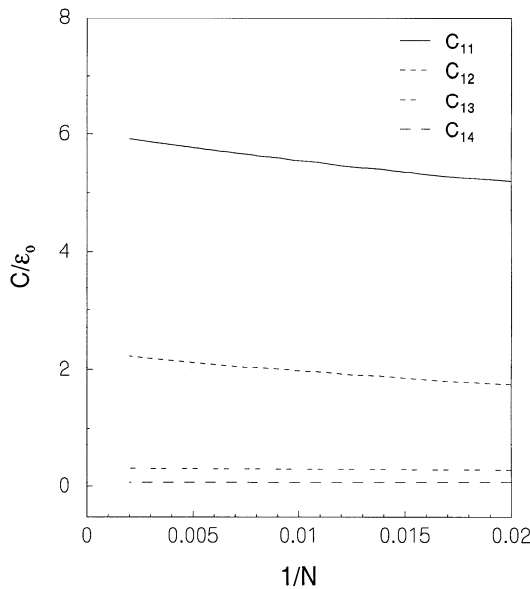

Figure 3. Convergence of the capacitances for the case of four conductor strip line ($\gamma = 180°$, $a_1 = 1.25$, $a_2 = 1.0$, spacing= 2°, strip widths= 20°, $\varepsilon_{r1} = 2.2$, $\varepsilon_{r2} = 4.7$).

Another way to establish confidence might be to look at the charge distribution on the conducting strips and on the two dielectric interfaces. Figure 4 shows the charge distribution plotted versus the angles

along the interfaces. The charge distribution computed by placing 1 Volt positive charge on the left strip and a 1 Volt negative charge on the right strip. As expected in the distribution a constant potential of +1 Volt appears on the left strip and a constant potential of -1 Volt appears on the left strip. Along the dielectric interface between the strips, the potential gradually changes from +1 Volt to -1 Volt. On the left and right sides the potential gradually drops to zero, because at these places the interfaces meet the perfectly conducting ground plane.
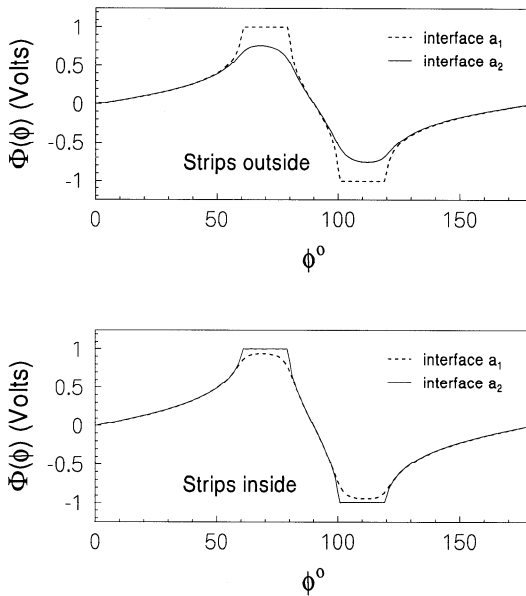
Figure 4. Charge distribution on the interfaces of the substrate and the overlay ($\gamma = 180°$, $a_1 = 1.25$, $a_2 = 1.0$, spacing= $2°$, strip widths= $20°$, $\varepsilon_{r1} = 2.2$, $\varepsilon_{r2} = 4.7$).

4.3. Modes on the multiconductor line

The number of modes existing on the transmission line depends upon the number of conductors. For each mode, there is an associated voltage eigenvector. The elements of the voltage eigenvector are the potentials associated with each conductor. For two symmetric conductors there are two modes called the even and odd modes, referring to the even and odd polarities of the voltage eigenvectors. For more than two

conductors the modes are simply labeled as numerical integers from 1 to S, where S is the number of conducting strips.

Each mode can be seen visually by plotting the electric field due to the potentials on the conductors (taken from the voltage eigenvectors) with the help of the program [5]. In Figures 5a and 5b the odd and even modes existing on a two conductor line are shown. The modes existing on a three conductor line are shown in Figures 6a to 6c. By looking at the voltage and current eigenvectors, it is found that the voltage and current on the second conductor is approximately zero. Since there is no voltage and current associated with the center conductor in mode 2, an impedance cannot be assigned to it either. Consequently no signal can travel through the center conductor in this mode. For the case of four conductors, the existing four modes are shown in Figures 7a to 7d.
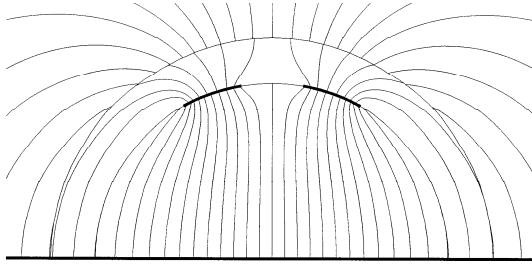

Figure 5a. The electric field for the even ($e_{11} = 8.500362, e_{12} = 8.500284$) mode existing on a two conductor strip line ($\gamma = 180°$, $a_1 = 1.25$, $a_2 = 1.0$, spacing= $20°$, strip widths= $20°$, $\varepsilon_{r1} = 2.2$, $\varepsilon_{r2} = 4.7$).
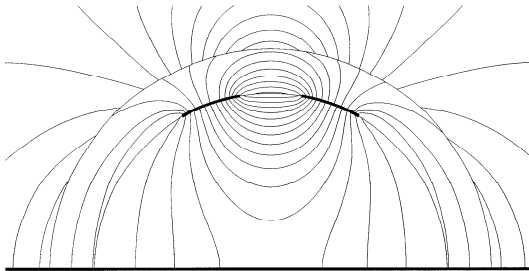

Figure 5b. The electric field for the odd ($e_{21} = 5.770987, e_{22} = -5.771112$) mode existing on a two conductor strip line ($\gamma = 180°$, $a_1 = 1.25$, $a_2 = 1.0$, spacing= $20°$, strip widths= $20°$, $\varepsilon_{r1} = 2.2$, $\varepsilon_{r2} = 4.7$).
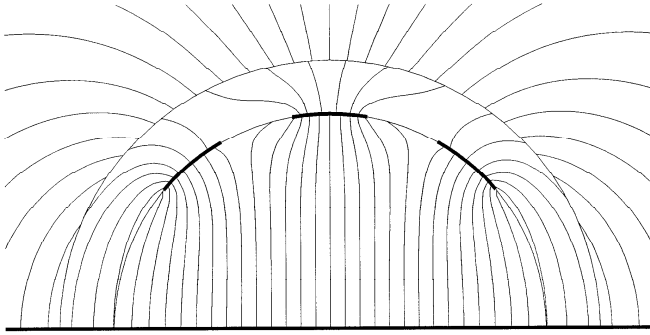
Figure 6a. The electric field for the mode 1 ($e_{11} = 6.676794, e_{12} = 8.507684, e_{13} = 6.676713$) existing on a three conductor strip line ($\gamma = 180°$, $a_1 = 1.25$, $a_2 = 1.0$, spacing= 20°, strip widths= 20°, $\varepsilon_{r1} = 2.2$, $\varepsilon_{r2} = 4.7$).
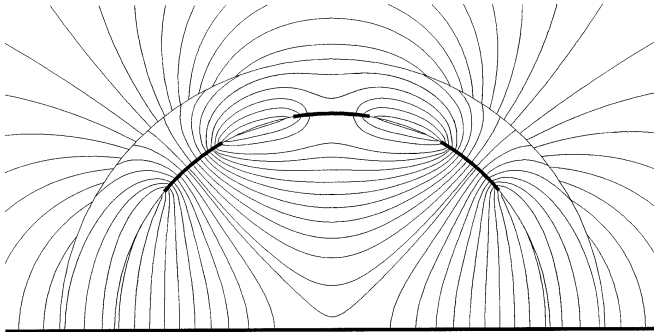

Figure 6b. The electric field for the mode 2 ($e_{21} = 6.386002, e_{22} = 2.490959E - 04, e_{23} = -6.386423$) existing on a three conductor strip line ($\gamma = 180°$, $a_1 = 1.25$, $a_2 = 1.0$, spacing= 20°, strip widths= 20°, $\varepsilon_{r1} = 2.2$, $\varepsilon_{r2} = 4.7$).
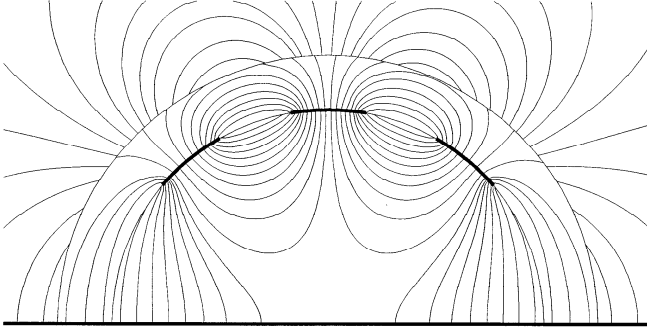
Figure 6c. The electric field for the mode 3 ($e_{31} = 3.572976, e_{32} = -5.809127, e_{33} = 3.572376$) existing on a three conductor strip line ($\gamma = 180°$, $a_1 = 1.25$, $a_2 = 1.0$, spacing= $20°$, strip widths= $20°$, $\varepsilon_{r1} = 2.2$, $\varepsilon_{r2} = 4.7$).
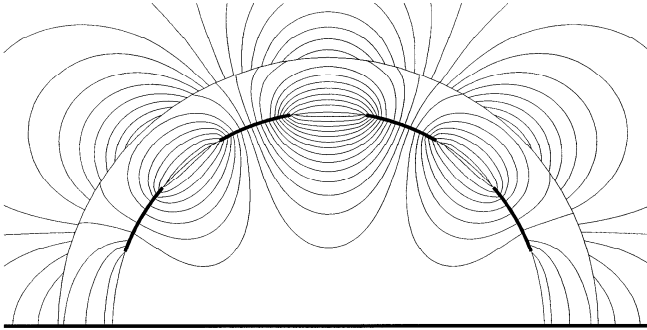

Figure 7a. The electric field for the mode 1 ($e_{11} = 2.990421, e_{12} = -4.377615, e_{13} = 4.371234, e_{14} = -2.978789$) existing on a four conductor strip line ($\gamma = 180°$, $a_1 = 1.25$, $a_2 = 1.0$, spacing= $20°$, strip widths= $20°$, $\varepsilon_{r1} = 2.2$, $\varepsilon_{r2} = 4.7$).
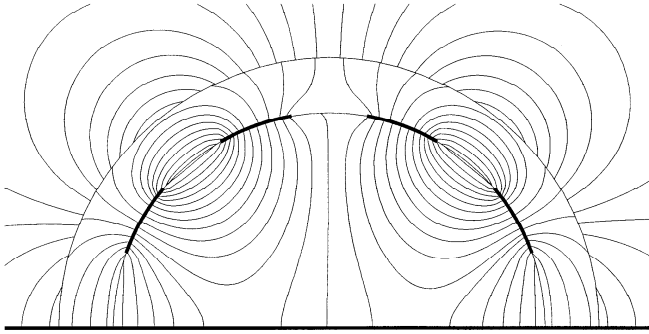
Figure 7b. The electric field for the mode 2 ($e_{21} = 4.933596, e_{22} = -2.815658, e_{23} = -2.823201, e_{24} = 4.944684$) **existing on a four conductor strip line** ($\gamma = 180°$, $a_1 = 1.25$, $a_2 = 1.0$, **spacing= $20°$, strip widths= $20°$,** $\varepsilon_{r1} = 2.2$, $\varepsilon_{r2} = 4.7$).
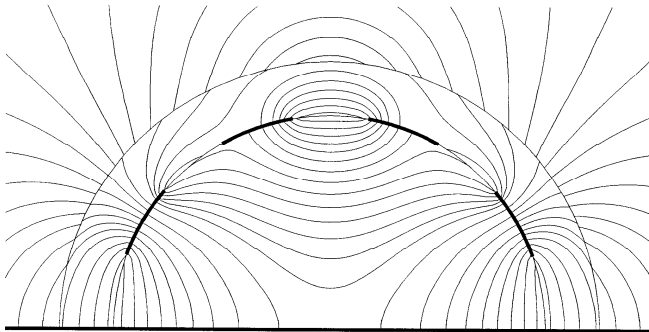

Figure 7c. The electric field for the mode 3 ($e_{31} = 5.453596, e_{32} = 3.726314, e_{33} = -3.728511, e_{34} = -5.449817$) **existing on a four conductor strip line** ($\gamma = 180°$, $a_1 = 1.25$, $a_2 = 1.0$, **spacing= $20°$, strip widths= $20°$,** $\varepsilon_{r1} = 2.2$, $\varepsilon_{r2} = 4.7$).
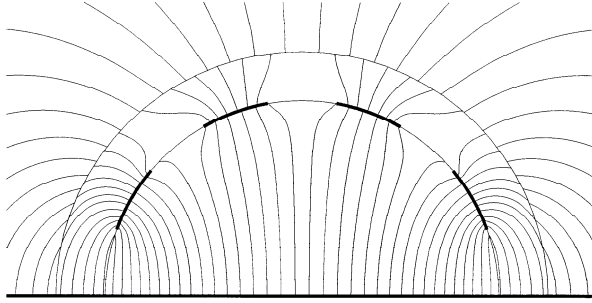
Figure 7d. The electric field for the mode 4 ($e_{41} = 4.428728, e_{42} = 7.895665, e_{43} = 7.895558, e_{44} = 4.428811$) **existing on a four conductor strip line** ($\gamma = 180°$, $a_1 = 1.25$, $a_2 = 1.0$, **spacing**$= 20°$, **strip widths**$= 20°$, $\varepsilon_{r1} = 2.2$, $\varepsilon_{r2} = 4.7$).

The same formulation of the problem can be used for studying the non-symmetric modes on the multiconductor line. As an example Figures 8a and 8b show the electric field distributions for the non-symmetric modes of the two conductor line (strips inside). The corresponding components of the two voltage eigenvectors are listed in the figure captions. It is seen that for the mode one, the voltages on the individual conductors are of the opposite polarity, but not exactly of the odd type. Likewise, the voltages corresponding to the mode two are of the same polarity, but not exactly even.
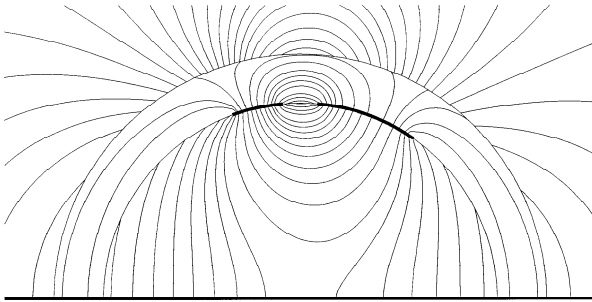

Figure 8a. The electric field for the non-symmetric mode 1 ($e_{11} = 3.999336, e_{12} = -6.805156$) **existing on a two conductor strip line** ($\gamma = 180°$, $a_1 = 1.25$, $a_2 = 1.0$, **spacing**$= 10°$, **strip widths**$= 15°$ **and** $30°$, $\varepsilon_{r1} = 4.7$, $\varepsilon_{r2} = 2.2$, **strips inside**).
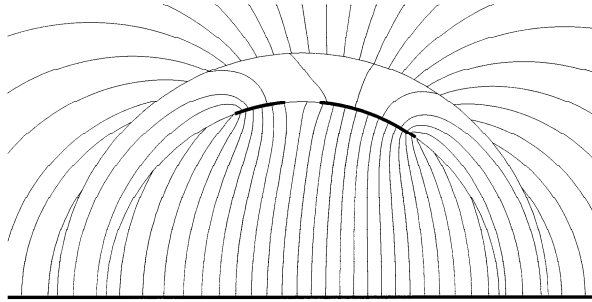
Figure 8b. The electric field for the non-symmetric mode 2 ($e_{21} = 9.492947, e_{22} = 9.088147$) **existing on a two conductor strip line** ($\gamma = 180°$, $a_1 = 1.25$, $a_2 = 1.0$, **spacing**$= 10°$, **strip widths**$= 15°$ **and** $30°$, $\varepsilon_{r1} = 4.7$, $\varepsilon_{r2} = 2.2$, **strips inside).**

4.4. Effects of the overlay and the substrate material

The effects of the dielectric material ϵ_{r1} of the overlay and ϵ_{r2} of the substrate on the transmission line characteristics was studied first. Figure 9 shows the normalized phase velocities versus the permittivity of the overlay, and the substrate for the case of four conductor strips. When the strips are placed inside, it was observed that the phase velocities for the different modes come closer to each other as ϵ_{r1} decrease from 20 to 1. For $\epsilon_{r1} = 1$ (air media), all the modes travel with the same phase velocity, a desirable effect in most signal transmission applications. The situation $\epsilon_{r1} = 1$ may be thought of as equivalent to the absence of the overlay when the strips been placed on one uniform dielectric material of radius a_2. When the strips are placed outside it was observed that the modes travel with the same phase velocity at the point where $\epsilon_{r1} = \epsilon_{r2}$. This condition may be considered equivalent to having the strips placed on just one uniform medium of radius a_1.

Figure 10 shows the phase velocities plotted versus the permittivity ϵ_{r2} of the substrate. When the strips are inside, the difference in phase velocities for all the existing modes reduces as ϵ_{r2} is increased. At about $\epsilon_{r2} = 10$ and above all the modes may be considered as traveling with the same phase velocity. The value of the overlay ϵ_{r1} also plays a part in how fast the phase velocities converge to one value. When the strips are outside, all the modes are traveling with the same phase velocity when ϵ_{r2} equals ϵ_{r1}.
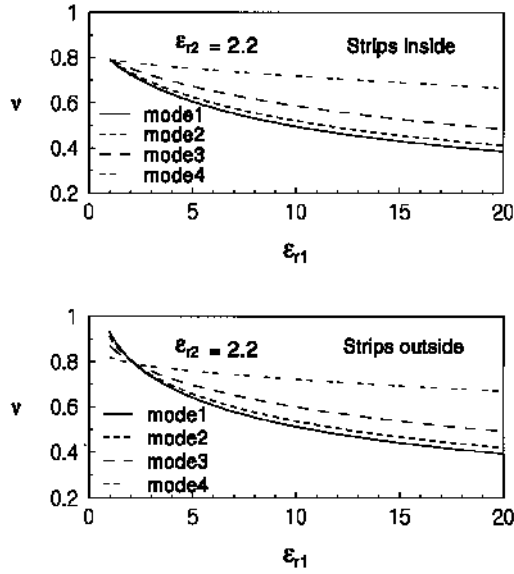
Figure 9. Phase velocities versus ε_{r1} for four conductor strip line ($\gamma = 180°$, $a_1 = 1.05$, $a_2 = 1.0$, spacing= $2°$, strip widths= $20°$).
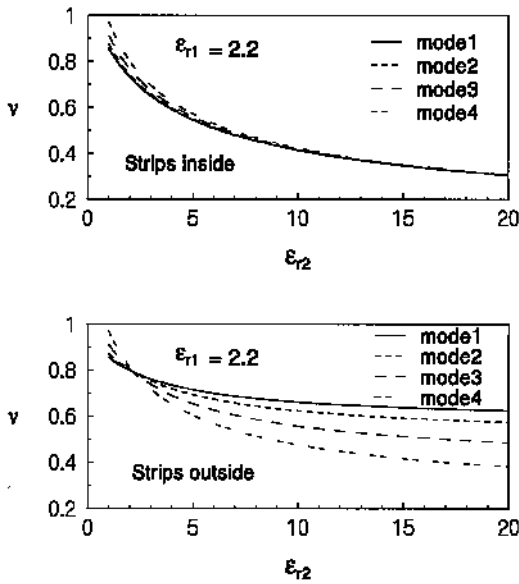

Figure 10. Phase velocities versus ε_{r2} for four conductor strip line ($\gamma = 180°$, $a_1 = 1.05$, $a_2 = 1.0$, spacing= $2°$, strip widths= $20°$).

The effects of varying the permittivity of the overlay on the coupling between the conductors of the transmission line was studied next. In case of two conductors, the coupling coefficient k_e in dB values is obtained from the voltage ratio V_2/V_1 when the line is terminated in a reflectionless load [6].

$$k_e = \frac{V_2}{V_1} = 20 \ \log_{10}[\frac{C_{12}}{C_{11} + C_{12}}] \tag{31}$$

Figure 11 shows the coupling coefficient versus ϵ_{r1} (overlay material) for the case of two conductor strips. Both for the strips outside and strips inside the coupling between the conductors becomes smaller as ϵ_{r1} decreases. It is desirable to have smaller coupling values for signal transmission purposes in order to reduce the crosstalk.
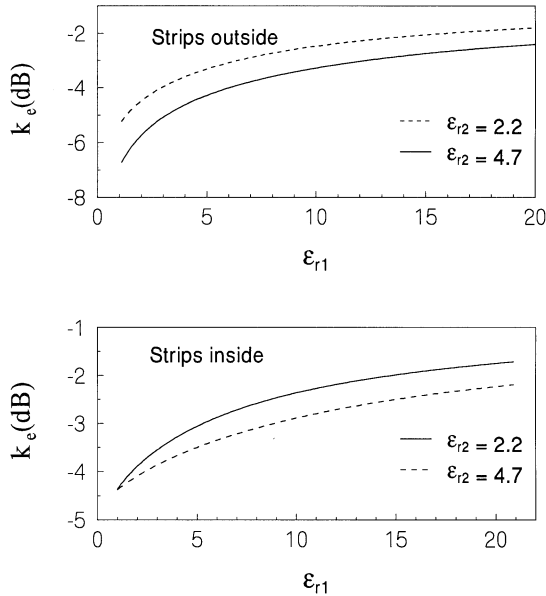

Figure 11. Coupling coefficient versus ε_{r1} **for two conductor strip line** ($\gamma = 180°$, $a_1 = 1.05$, $a_2 = 1.0$, **spacing= 2°, strip widths= 20°, strips outside and strips inside).**

Figure 12 shows the coupling coefficient plotted versus the permittivity of the substrate ϵ_{r_2} for the case of two conducting strips. For the strips placed inside, the coupling is almost unaffected by the presence of the material media of the substrate, while for the strips placed outside, the coupling between the two conductors becomes weaker as the permittivity of the substrate increases. Thus by placing the strips on top of the overlay, the coupling between the conductors can be controlled by adjusting the permittivity of the substrate. When there are more than two conductors we will use the normalized mutual capacitances as the parameter to represent the coupling between the conductors. In case of symmetric configurations of three and four conducting strips the stronger coupling capacitances (C_{12} in case of three strips and C_{12} and C_{23} in case of four strips) increased directly with ϵ_{r1} and plays an important part in the crosstalk effect [8].
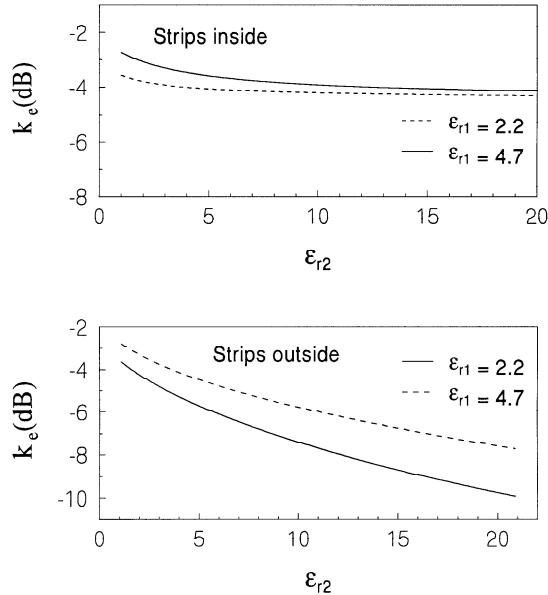

Figure 12. Coupling coefficient versus ε_{r2} for two conductor strip line ($\gamma = 180°$, $a_1 = 1.05$, $a_2 = 1.0$, spacing= 2°, strip widths= 20°, strips outside and strips inside).

Figure 13 shows the coupling capacitances plotted versus the permittivity of the substrate for the cases of three conducting strips. In this case a slightly different observation is made. For the outside strips, the coupling capacitances have low values and slowly increase with ϵ_{r2}, while for the inside strips, the coupling capacitances grow relatively faster with ϵ_{r2}. Hence in contrast to the two-conductor case, the coupling can be controlled by placing the strips between the substrate and the overlay and adjusting the permittivity of the substrate. Similar observation for the four strips is reported in [8].
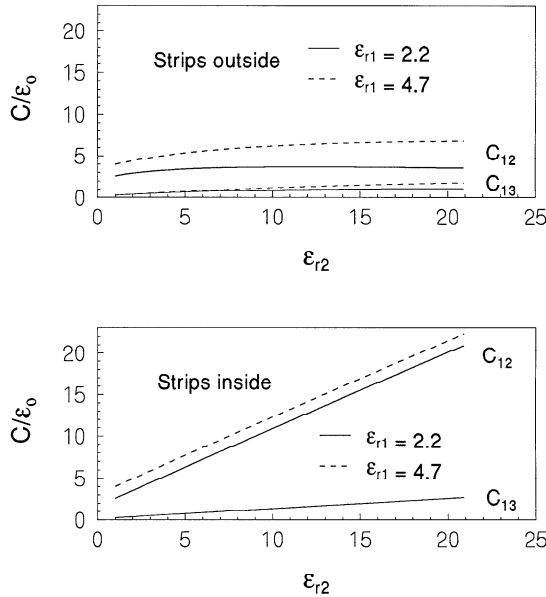

Figure 13. Coupling capacitances versus ε_{r2} for three conductor strip line ($\gamma = 180°$, $a_1 = 1.05$, $a_2 = 1.0$, spacing= $2°$, strip widths= $20°$, strips outside and strips inside).

4.5. Effects of the spacing between the strips

To study the effects of spacings between the conducting strips, the relative permittivities of the substrate and the overlay are set constant at 4.7 and 2.2, respectively. The width of the strips is kept constant at $20°$. The line parameters such as the phase velocity and coupling are then examined one by one as the spacing between the conducting

strips is varied. In Figure 14, the phase velocities and the coupling capacitances are plotted versus the angle $(\alpha_{i+1} - \beta_i)^\circ$ which is the spacing between the strips for the case of symmetric three conductor line. It can be seen that the difference in phase velocities is much smaller for the inside strips as compared to the outside strips. The coupling for both the strips outside and strips inside decreases as the spacing between the strips increases. Similar observations were made for the phase velocity and coupling results for the cases of two and four conductor strip lines [8].
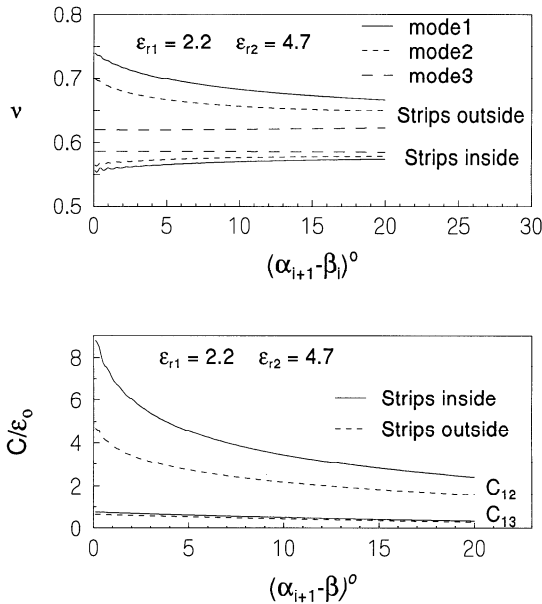

Figure 14. Phase velocities and coupling capacitances versus $(\alpha_{i+1} - \beta_i)^\circ$ (spacing between the strips), for three conductor strip line ($\gamma = 180^\circ$, $a_1 = 1.05$, $a_2 = 1.0$, spacing= 2°, strip widths= 20°, $\varepsilon_{r1} = 2.2$, $\varepsilon_{r2} = 4.7$, strips outside and strips inside).

4.6. Effects of the strip widths

The effect of having different strip widths on the line parameters was studied next. The spacing between the strips is now kept constant at 2° apart. The relative permittivities of the substrate and the overlay are set to 4.7 and 2.2, respectively. The phase velocities and coupling

capacitances are plotted versus $(\beta_i - \alpha_i)^\circ$ in Figure 15, for the case of three conductor strips. It is noticeable that the phase velocities for the different modes are much closer to each other for the inside strips than for the outside strips. This means less distortion at the end of the line when strips are placed between the substrate and the overlay. As would be intuitively expected, the capacitance between conductors becomes weaker for smaller strip widths and grows stronger as the strip widths increase. A similar observation was made of the phase velocity and coupling for the cases of two and four conductor strip lines [8].
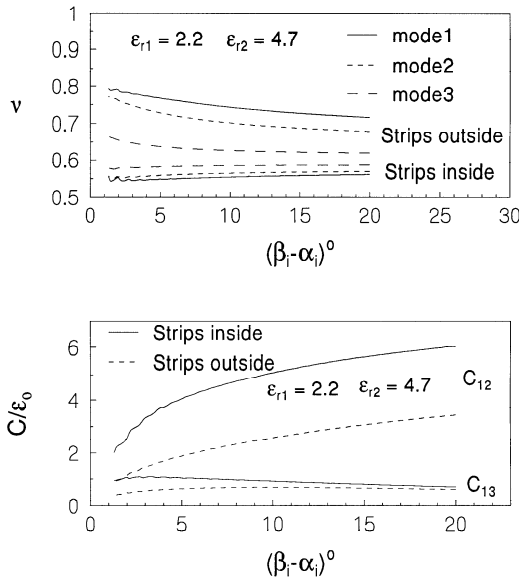

Figure 15. Phase velocities and coupling capacitances versus $(\beta_i - \alpha_i)^\circ$ (strip widths), for three conductor strip line ($\gamma = 180^\circ$, $a_1 = 1.05$, $a_2 = 1.0$, spacing$= 2^\circ$, $\varepsilon_{r1} = 2.2$, $\varepsilon_{r2} = 4.7$, strips outside and strips inside).

4.7. Effects of the overlay thickness

In further study, the overlay radius a_1 is varied from 1 to 2, while the substrate radius a_2 is kept constant at 1. The strip widths and the spacing between the strips are set constant at 20° and 2°, respectively. The relative permittivities of the substrate and the overlay are set constant at 4.7 and 2.2, respectively. The line parameters are then examined as the ratio a_1/a_2 is varied.

In Figure 16, the phase velocities are plotted versus the thickness ratio a_1/a_2 for the three conducting strips case. For the strips placed inside, the least difference in phase velocities depends not only on the thickness of the overlay but also on the permittivity of the overlay. As the thickness of the overlay increases the difference in phase velocities decreases. Also, the smaller the permittivity of the overlay, the less is the difference in phase velocities. On the other hand, for the outside strips, the least difference in phase velocities occurs when the thickness of the overlay is increased and when the permittivities of the substrate and the overlay become similar to each other. The same behavior was observed for the cases of two and four conductor strip lines [8].

The coupling capacitance is shown plotted versus the thickness of the overlay in Figure 17 for the case of the three conducting strips. One thing that can be observed from this case (and also for two and four conductor strips) that the coupling depends more on the permittivity of the overlay than on the thickness of the overlay. However the coupling does reduce as the thickness of the overlay is increased. The second observation is that the outside strips have lower coupling values as compared to inside strips.
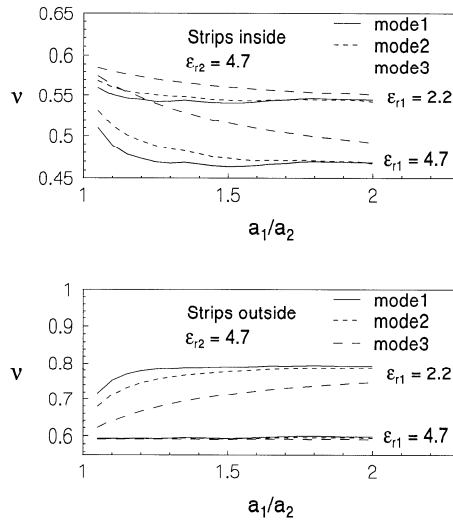

Figure 16. Phase velocities versus a_1/a_2 (overlay thickness), for three conductor strip line ($\gamma = 180°$, $a_2 = 1.0$, spacing= $2°$, strip widths= $20°$, $\varepsilon_{r2} = 4.7$, strips outside and strips inside).
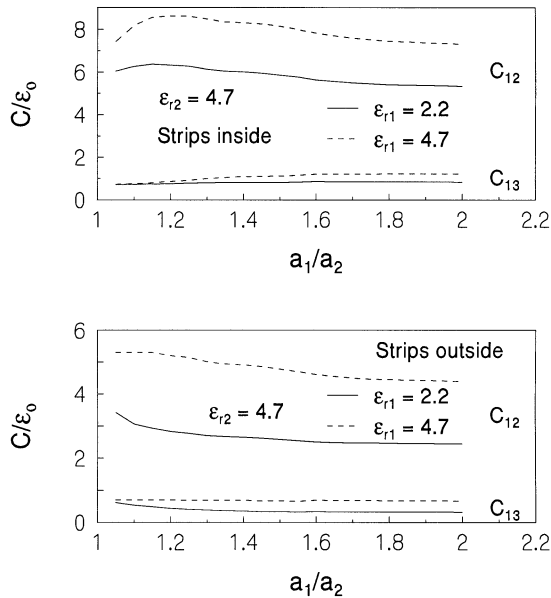
Figure 17. Coupling capacitances versus a_1/a_2 (overlay thickness), for three conductor strip line ($\gamma = 180°$, $a_2 = 1.0$, spacing= $2°$, strip widths= $20°$, $\varepsilon_{r2} = 4.7$, strips outside and strips inside).

4.8. Effects on the mode impedances

In order to design good matching networks, it is essential to know how the mode impedances behave subjected to different material and geometrical properties of the multiconductor transmission line. To accomplish this objective the material and dimensional properties of transmission line are discussed in detail in [8]. Here a couple of these results are discussed briefly. In Figures 18 and 19 the mode impedances from (30) are shown plotted versus the strip widths for four conducting strips. It is observed that in all the modes the impedances grow larger as the widths of the strips becomes smaller. While on the other hand, wider strips give low impedance values. In addition, the strips placed outside exhibit higher impedance values as compared with the strips placed inside.
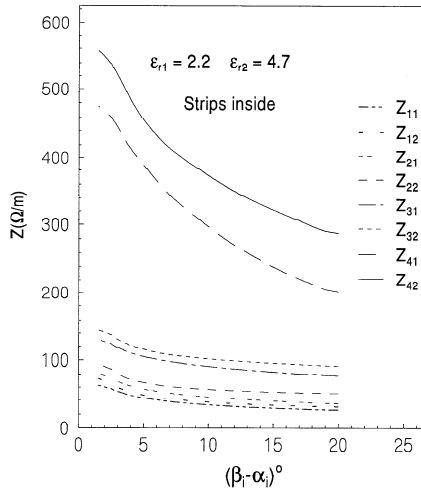
Figure 18. Mode impedances versus $(\beta_i - \alpha_i)^\circ$ (strip widths), for four conductor strip line ($\gamma = 180^\circ$, $a_1 = 1.05$, $a_2 = 1.0$, spacing$= 2^\circ$, strip widths$= 20^\circ$, $\varepsilon_{r1} = 2.2$, $\varepsilon_{r2} = 4.7$, strips inside),
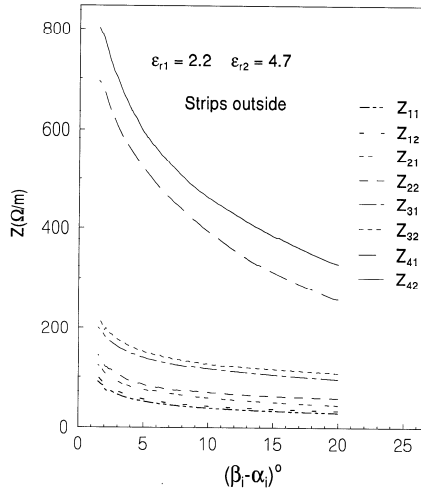

Figure 19. Mode impedances versus $(\beta_i - \alpha_i)^\circ$ (strip widths), for four conductor strip line ($\gamma = 180^\circ$, $a_1 = 1.05$, $a_2 = 1.0$, spacing$= 2^\circ$, strip widths$= 20^\circ$, $\varepsilon_{r1} = 2.2$, $\varepsilon_{r2} = 4.7$, strips outside).

5.   Summary and Conclusion

There were two basic objectives of analyzing the multiconductor cylindrical transmission line system. The first of them was to investigate conditions under which the transmission line exhibited the least phase distortion, that is, signals on the different conductors travel with almost the same phase velocity. The second one was how to make the transmission line immune to a crosstalk, that is, to minimize the coupling between conductors.

Looking at the material properties of the substrate and the overlay, the following conclusions were made about the phase velocities and the coupling on the line. The least difference in phase velocities occurred when the overlay was replaced with air media (strips inside) and when the permittivity of the substrate and the overlay were the same (strips outside). These two situations may be considered equivalent to having the strips placed on top of one uniform dielectric material layer (i.e. no overlay). In general, if two dielectric layers are used then the least difference in phase velocities occurred when the relative permittivity of the substrate is kept as high as possible (10 or above) and the relative permittivity of the overlay as low as possible (close to 1). The coupling in case of two conductors was reduced considerably by selecting the substrate material of high permittivity and the overlay material of low permittivity. In contrast to the two conductor case, for the three and four conductor strips, low coupling values were obtained when both the substrate and the overlay had low permittivity values. In general, the coupling between the conductors could be reduced by placing the strips outside of the overlay instead of placing them between the substrate and the overlay.

Looking at the dimensional properties of the transmission line, the following conclusions were made about the phase velocities and the coupling on the line. In general, the least difference in phase velocities occurred when the strips were placed between the substrate and the overlay as compared to the strips placed outside of the overlay. Furthermore, by increasing the thickness of the overlay, the widths of the strips and the spacing between the strips, the difference in the phase velocities could be reduced. In contrast to the phase velocities, low coupling values are obtained when the strips are placed outside of the overlay as compared to the strips placed between the substrate and the overlay. Furthermore, by increasing the thickness of the

overlay, the spacing between the strips and decreasing the strip widths, the coupling between the conductors could be reduced.

Finally, the impedance curves provide the practical limits for the selection of the material (permittivities of the layers) and dimensional parameters (thickness of the overlay, strips widths and spacing between the strips) of the cylindrical transmission line.

Acknowledgments

References

1. Auda, H. A., "Cylindrical microstrip line partially embedded in a perfectly conducting ground plane," *IEEE Trans. Microwave Theory Tech.*, Vol. 39, 1662–1666, Sept. 1991.
2. Auda, H. A., and A. Z. Elsherbeni, "Multiple microstrip lines in a multilayered cylindrical dielectric substrate on perfectly conducting wedge," *IEEE Trans. Microwave Theory Tech.*, Vol. 41, 1037–1042, July 1993.
3. Kajfez, D., *Notes on Microwave Circuits*, 2, Oxford, MS, Kajfez Consulting, 1986.
4. Mattaei, G. L., L. Young, and E. M. T. Jones, *Microwave Filters, Impedance-Matching Networks, and Coupling Structures*, New York, McGraw-Hill, 1964.
5. Kajfez, D., K. Mahadevan, and J. A. Gerald, "PC Software maps electromagnetic vector fields," *Microwave Journal*, Vol. 32, 267–280, May 1982.
6. Hoffmann, R. K., *Handbook of Microwave Integrated Circuited*, Norwood, Artech House, Chapter 9, 1987.
7. Stratton, J. A., *Electromagnetic Theory,* New York, McGraw-Hill, 1941.
8. Elsherbeni, A. Z., O. D. Khan, C. E. Smith, and D. Kajfez, "Analysis of a class of cylindrical microstrip transmission lines," *Technical Report 95-3*, Department of Electrical Engineering, University of Mississippi, October 1995.